APPLICATIONS OF NEAR FIELD OPTICAL MICROSCOPY :

Fluorescence in situ hybridisation, Langmuir-Blodgett films and integrated optical waveguides.

NIEK VAN HULST, MARCO MOERS & ERIK BORGONJEN
Applied Optics group, Faculty of Applied Physics
& MESA Research Institute,
University of Twente,
P.O.Box 217, 7500AE Enschede, the Netherlands.

Abstract

Scanning Near-field Optical Microscopy (SNOM), based on metal coated adiabatically tapered fibres, combined with shear force feedback and operated in illumination mode, has proven to be the most powerful SNOM arrangement, because of its true localisation of the optical interaction, its true optical contrast (fluorescence, polarisation, etc.) and its sensitivity down to the single molecular level. We present the first application of SNOM to (i) Fluorescence *In Situ* Hybridisation (FISH) of human metaphase chromosomes, where the localised fluorescence allows to identify specific DNA sequences in addition to the topographic force image, and (ii) Langmuir-Blodgett mono-layers, where the orientation of the polymer backbone and the degree of polymerisation is visualised in the near-field polarised fluorescence simultaneously with the topography in the force signal.

Photon Scanning Tunnelling Microscopy (PSTM), based on frustration of total internal reflection with uncoated dielectric probes and operated in transmission mode, is experimentally easier than aperture SNOM, but less straightforward in its interpretation as generally near field and far field scattering are observed mixed with topographic effects. We have applied combined PSTM/AFM to (i) Langmuir-Blodgett mono-layers, and (ii) integrated optical ridge waveguides. Both systems have virtually no surface structure. In the waveguides purely the electric field distribution is probed by coupling to the evanescent wave. Direct observation by PSTM of TM and TE modal field distributions, mode beating and application to a Y-junction wavelength (de)multiplexer is presented.

O. Marti and R. Möller (eds.), Photons and Local Probes, 165–180.

1. Introduction

Near field optical microscopy has gone through some essential developments since the first demonstration of super-resolution by Pohl *et al.* [1]. Especially the combination of adiabatic fibre pulling, as introduced by Betzig *et al.* [2,3], and shear force feedback (Toledo-Crow *et al.* [4], Betzig *et al.* [5]) has resulted in a reproducible, relatively efficient aperture probe, which can be operated non-destructively. Using these probes application of near field fluorescence microscopy to biological and chemical samples was recently explored (Betzig *et al.* [6], Moers *et al.* [7]). A major step was set by Betzig and Chichester [8] in the observation of single molecular fluorescence using a pulled fibre probe, directly followed by single molecular spectroscopy (Trautman *et al.* [9]), quantised luminescence (Hess *et al.* [10]) and picosecond single molecular dynamics (Sunney Xie *et al.* [11], Ambrose *et al.* [12]). Clearly the virtues of optics, high spectral resolution, orientational sensitivity and high time resolution, all apply to the near field domain with its high spatial resolution, which adds extensively to the potential of scanning probe microscopy. In this paper we present first results on some new applications of combined near field optical and force microscopy, using both aperture type and dielectric probes.

2. Aperture probe applications

2.1. MICROSCOPE SET-UP

Our near field optical microscope is designed specifically for application to chemical and biological samples [13]. The microscope allows the use of standard microscope object glasses and viewing of the sample by a high NA objective (0.7 NA dry or 1.4 NA immersion oil) which is important for localisation of specific biological samples and efficient collection of fluorescence. The basis of the set-up is a Zeiss axiovert 135TV inverted microscope which was chosen for its high mechanical stability, i.e. three point support of the sample table, and high efficiency of the optical light paths. The inverted microscope rests on an optical table with passive vibration isolation. The sample table was replaced by a home built table with mechanical sample translation using multimorph piezo translators (NEC, type AE0203D08) with 7 μm scan range. The near field part of the microscope is schematically shown in Figure 1. The probe is fabricated by adiabatic tapering of an optical fibre using a commercially available fibre puller (Sutter P2000) and subsequent directional coating with aluminium. About 5 mW laser light of an Ar^+-/Kr^+-laser (Coherent, Innova 70 Spectrum) is coupled into the fibre, where the incident polarisation can be rotated using a $\lambda/4$ and a polarisation plate. Typically 1 nW is emitted into the far field for an aperture of ~ 80 nm. The far field signal is collected by a high NA objective. Several exit ports are accessible, accommodating eyepieces, a CCD camera and a point detector. For fluorescence detection a dichroic mirror and long-pass filter are used, which block the excitation light. In near field operation the probe source is confocally imaged onto the point

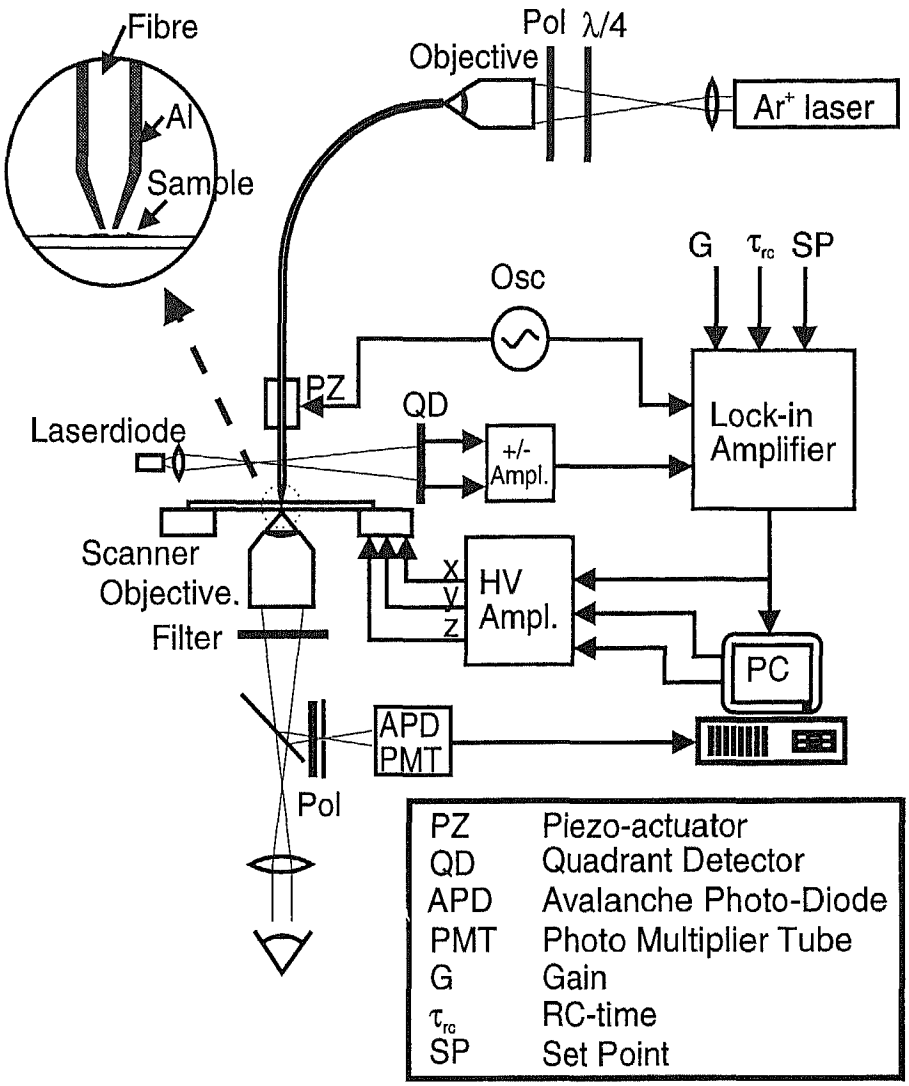

Figure 1. Schematic set-up of the aperture type scanning near-field optical microscope (SNOM) with metallized adiabatically tapered fibre (inset), scanned sample stage on an inverted optical microscope (Zeiss axiovert 135TV), shear force feedback on tip sample distance, excitation by Ar^+-/Kr^+-laser (Coherent, Innova 70 Spectrum), detection via NA 0.7 objective by a photo-multiplier tube (PMT, Hamamatsu R1463-01) or photon counting avalanche photo-diode (APD, EG&G SPCM 2000) and polarising optics [7,13].

detector. For high light levels, > 1 fW, a photo-multiplier tube (PMT, Hamamatsu R1463-01) is used in combination with a 200 μm pinhole in the image plane. For low light levels a 150 μm area photon counting avalanche photo-diode (APD, EG&G SPCM200) is used with ~ 60 % quantum efficiency and ~ 5 dark counts/sec. While scanning the distance between probe and sample surface is kept constant at about 3 nm by a feedback system based on shear force detection [4,5]. Hereto the fibre probe is attached to a piezo-electric element which oscillates the fibre with an amplitude of about 30 nm at its resonance frequency (typically 10 kHz) in the lateral direction, i.e. parallel to the sample surface. The oscillation amplitude is measured with a sensitivity of ~ 1 nm by illuminating the fibre with a laser diode (λ = 780 nm) and detecting the diffraction pattern on a quadrant detector. The difference signal of the proper quadrants is amplified and fed to a lock-in amplifier. On approaching the sample surface the lock-in signal decreases due to "shear" forces between tip and sample. The physical origin of these forces is still subject of further study, yet their presence allows the operation of a feedback loop at an effective shear force value (set point). The RC-time of the loop is 1 to 10 msec. The correction signal is fed to the z-piezo element in the scanner and gives simultaneously the sample height. Both optical and height signal are digitised and stored in a personal computer, which also generates the scan pattern and timing for photon counting.

2.2 LANGMUIR-BLODGETT FILMS.

A monolayer of diethylene glycol diamine pentacosa-diynoic amide (DPDA) was investigated [7]. The layer was prepared by the Langmuir-Blodgett technique, polymerised by UV radiation and transferred to a microscope object glass [14]. The polymerised DPDA monolayer is 6 nm high with strong absorption around λ = 500 nm and fluorescence at λ = 550 - 600 nm. Moreover, depending on the lateral pressure during polymerisation and the transfer procedure, several domains are formed with a wide range of dimensions.Figure 2 shows a 4 x 4 μm^2 scan of the DPDA film. In the shear force image, Figure 2a, several domains and the underlying glass substrate are visible. Figure 2b and 2c show the corresponding near field fluorescence images with mutually perpendicular directions of incident polarisation. The excitation is at the 514 nm Ar^+-line and the fluorescence is detected at λ > 590 nm. Peak value of the fluorescence intensity is about 1 fW. Comparison of these images clearly demonstrates the advantage of near field optics in combination with force microscopy. The force image shows the presence of monolayer domains with a lateral resolution of ~ 30 nm. The fluorescence images show the high anisotropy of the polymerised diacetylenic films with ~ 100 nm lateral resolution: domains fluorescent for one polarisation direction are dark for the perpendicular direction and vice versa. The absorption and emission dipole moments of polydiacetylenes are oriented parallel to the polymer backbone, where the orientation is uniform over each domain due to the crystallinity of the Langmuir-Blodgett film. Thus from the near field optical images the orientation of the polycarbon backbone and the efficiency of the polymerisation can be determined, additional to the topography from the simultaneously recorded force image.

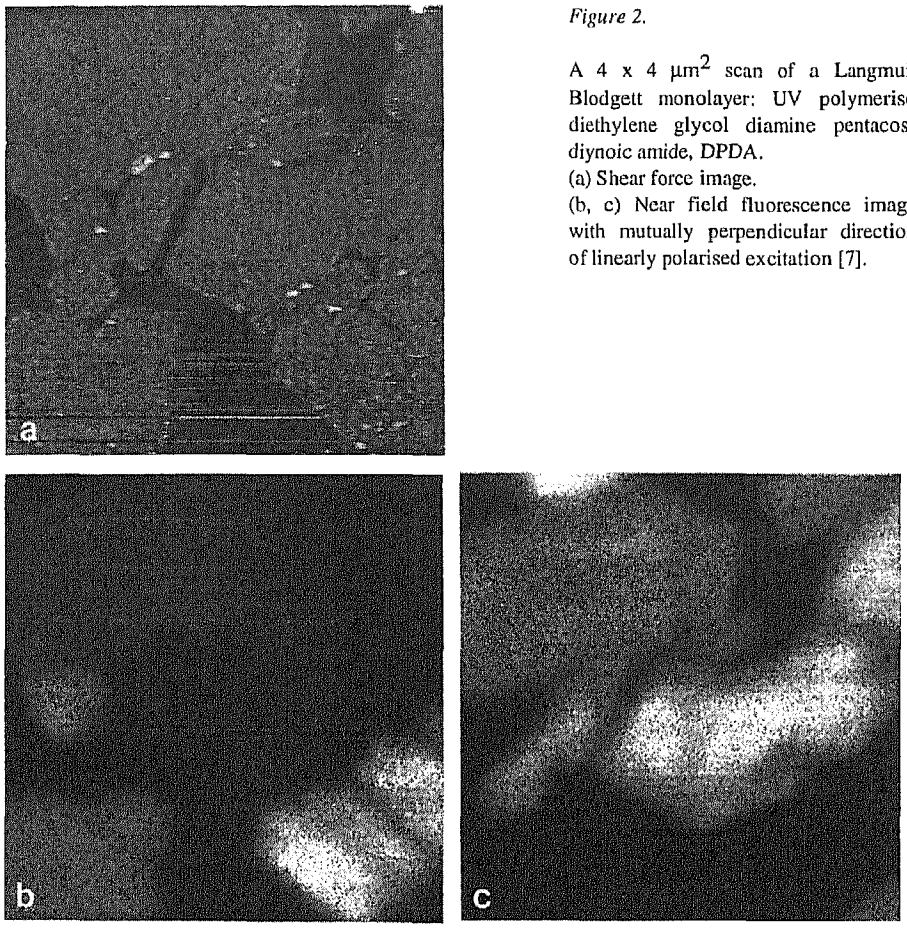

Figure 2.

A 4 x 4 μm^2 scan of a Langmuir-Blodgett monolayer: UV polymerised diethylene glycol diamine pentacosa-diynoic amide, DPDA.
(a) Shear force image.
(b, c) Near field fluorescence images with mutually perpendicular directions of linearly polarised excitation [7].

2.3. FLUORESCENCE *IN SITU* HYBRIDISATION

Over the last decade the technique of fluorescence *in situ* hybridisation (FISH) has developed as one of the major cytogenetic detection methodologies for human genetics [15,16]. Using fluorescent labels, FISH enables direct visualisation of topological or positional information of gene sequences under a fluorescence microscope. Thus FISH allows rapid localisation of genomic DNA fragments and identification of chromosomes with a superior resolution and signal-to-noise ratio compared to radioactive *in situ* hybridisation and chromosome banding techniques. Typically a resolution better than 10^6 basepairs can be obtained using (pro)metaphase chromosomes [17]. Yet the localisation of the fluorescence labels is fundamentally

limited by diffraction in conventional fluorescence microscopy, as schematically indicated in Figure 3. Recently Putman *et al.* [18] have shown that further improvement can be obtained using force microscopy to detect the morphological features of the *in situ* hybridisation label after enhancement to about 100 nm by an enzyme cytochemical reaction. Yet fluorescence detection has the advantage of higher specificity and moreover multicolour labelling can be applied [17]. We anticipated that the superior lateral resolution of near field fluorescence might allow improved localisation of the labels while maintaining the potential of multicolour labelling, provided the labels are sufficiently close to the chromosomal surface and the fluorescence level is still detectable. Some preliminary results are presented.

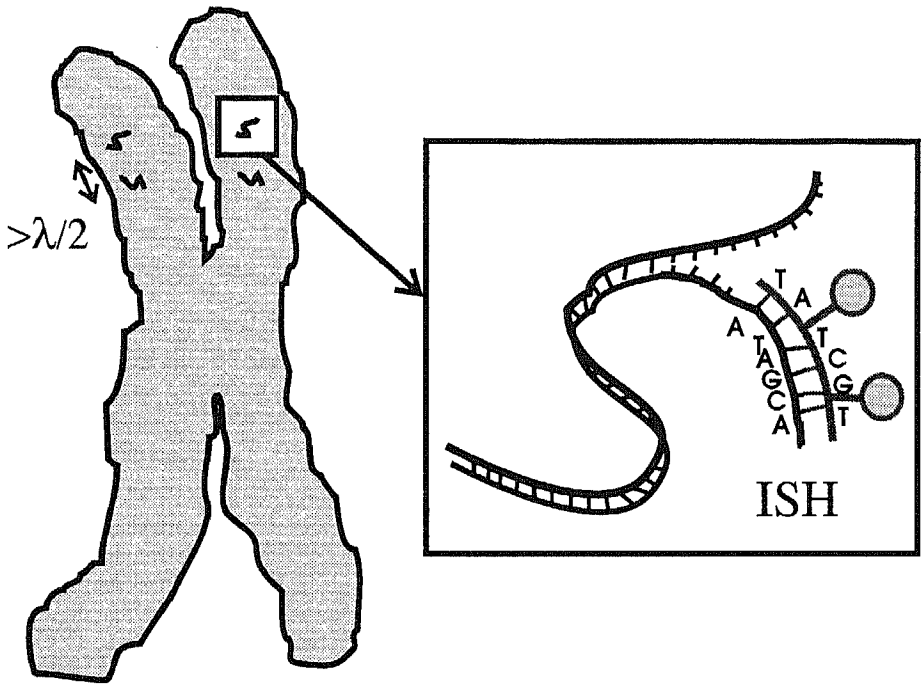

Figure 3. Principle of fluorescence *in situ* hybridisation. A fluorescent label is bound to a specific DNA sequence of a chromosome in the metaphase. The resolution of the fluorescence localisation determines the accuracy of gene sequencing.

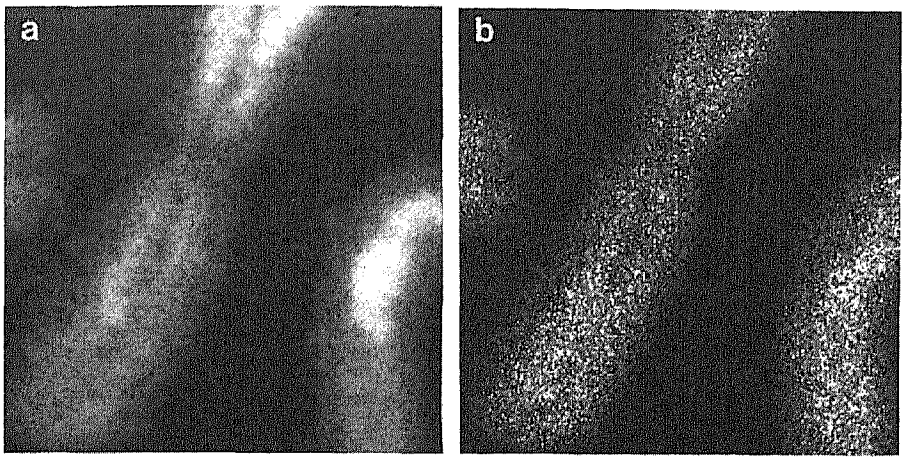

Figure 4. A 5 x 5 μm^2 scan of metaphase chromosomes (Chinese hamster lung). (a) Shear force image displaying the topography and (b) near field fluorescence image displaying non-specific propidium-iodide (PI) staining.

Figure 4 shows a typical result on metaphase chromosomes, isolated from Chinese hamster lung cells (V78), using standard procedures for optical microscopy. The chromosomes are air-dried on an object glass. The shear force image (Fig. 4a) displays the topography with a lateral resolution of ~ 50 nm, showing the separation of the chromatides, with a height of ~ 100 nm, and some DNA material on the glass substrate surrounding the chromosome. The corresponding near field fluorescence image (Fig. 4b) displays a non-specific staining by propidium-iodide (PI), showing complete correlation with the topography, including the chromatide separation. The scan is 200 x 200 pixels with 25 msec/pixel, peak fluorescence level is 68 cnts/pixel and avarage background is 3 cnts/pixel.

Figure 5 shows a scan of human metaphase chromosome #1 with specific labelling of the centromeric area (CY3-p1 fluorophore) by *in situ* hybridisation. In the shear force image (Fig. 5a) the high spatial frequency filtered piezo feedback signal is displayed, which again shows the chromosome topography with some substructure. The corresponding near field fluorescence image (Fig. 5b) displays the green fluorescence at $\lambda > 570$ nm, using BG39 and KV550 Schott filters, with excitation by the 568 nm Kr^+-line. The image is 200 x 200 pixels with 25 msec/pixel. The speckled background in the fluorescence image reflects the discrete level of 0 to 3 cnts/pixel. The specific labelling of the centromeric chromosome area is clearly visible with 60 to 120 cnts/pixel fluorescence. Beside the chromosome are some locally fluorescent areas due to unbound fluorophore. Based on the signal level ($\leq$ 10 cnts/pixel) we estimate ~ 10 fluorescent molecules to be present in these spots. The full width of these spots is about 150 nm, which is an indication for the optical resolution.

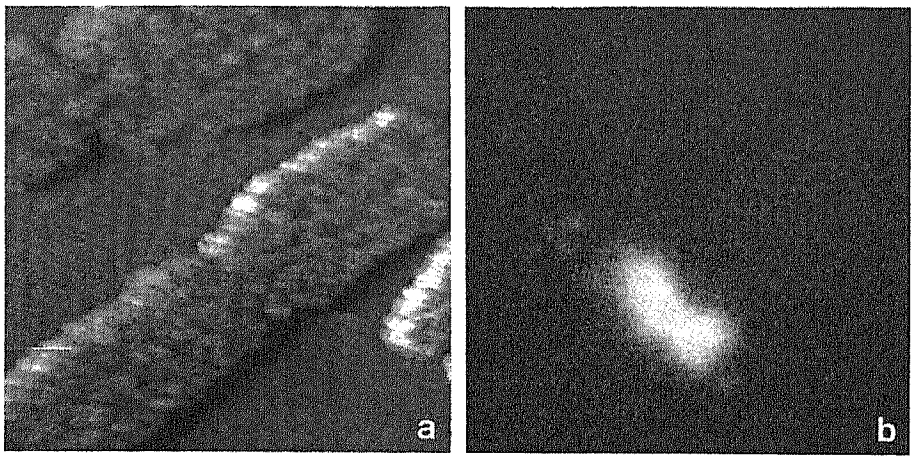

Figure 5. A 7 x 7 μm^2 scan of human metaphase chromosome #1. (a) Shear force image, high spatial frequency filtered and (b) near field fluorescence image displaying specific labelling of the centromeric area with CY3 fluorophore by *in situ* hybridisation.

3. Dielectric probe applications

3.1. MICROSCOPE SET-UP

In photon scanning tunneling microscopy (PSTM) a sharp dielectric probe is used for local conversion of an evanescent wave into a propagating wave. In our PSTM we use a micro-fabricated silicon-nitride (SiN) probe, which is commercially available (Park Scientific Instruments) for conventional AFM applications. For near field optical applications the SiN probe is a suitable high-index optical structure with 20 - 50 nm apex and transparency down to $\lambda = 290$ nm. Due to the integrated cantilever the probe can be scanned in close contact with a sample surface with feedback regulation on the force interaction. Generally the gold coating on the commercial cantilevers is removed for PSTM operation. In some applications the probe is sharpened further to ~ 10 nm by *e*-beam deposition. The sample is placed on a BK7 glass substrate and illuminated by a weakly focused laser beam (10 mW on ~ 100 μm) at an angle larger than the critical angle for total internal reflection, see Figure 6. The light generated by frustration of the evanescent wave at the SiN apex, ~ 1 nW, is collected by conventional optics. The deflection of the cantilever is detected using a standard optical beam deflection configuration. While scanning the interaction force is kept constant by a feedback on the beam deflection signal, yielding simultaneously a topographic and a near field optical image [19,20].

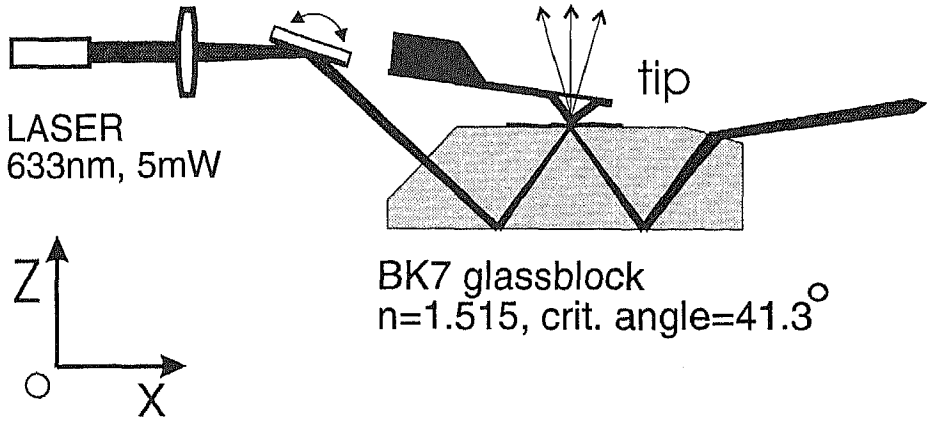

Figure 6. Schematic set-up of the photon scanning tunneling microscope (PSTM) based on localised frustration of total internal reflection by a micro-fabricated silicon-nitride (SiN) probe [19,20].

3.2. LANGMUIR-BLODGETT FILMS

A UV polymerised Langmuir-Blodgett film of 10,12-pentacosa-diynoic-acid (PCA) was investigated. After transfer to a glass substrate these PCA films display uniform domains with a height of 6 nm and a wide range of lateral dimensions. The domains show strong absorption bands at $\lambda = 505$ and 555 nm and fluorescence around $\lambda = 562$ and 640 nm, where absorption and emission dipole moment are along the highly oriented polycarbon backbone.

A combined PSTM/AFM scan of a 1 x 1 μm^2 area PCA film is shown in Figure 7. The AFM image (Fig. 7a) displays the z-piezo signal in feedback mode, showing mainly the monolayer topography with 6 nm height. The corresponding PSTM image (Fig. 7b) displays the fraction of the incident p-polarised light at $\lambda = 514$ nm which is coupled out via the SiN probe. Monolayer domains are clearly visible in the PSTM image, with an edge steepness of 30 nm, far beyond the diffraction limit. The PSTM signal on the domains is 10% below the signal detected on the surrounding glass, which is in agreement with the measured absorption of a PCA monolayer at 514 nm by far field methods. Consequently the PSTM contrast is mainly caused by absorption for this sample. Yet it should be noted that the expected polarisation anisotropy could not be observed. Also the observed fluorescence turned out *not* to be confined to the probe dimensions.

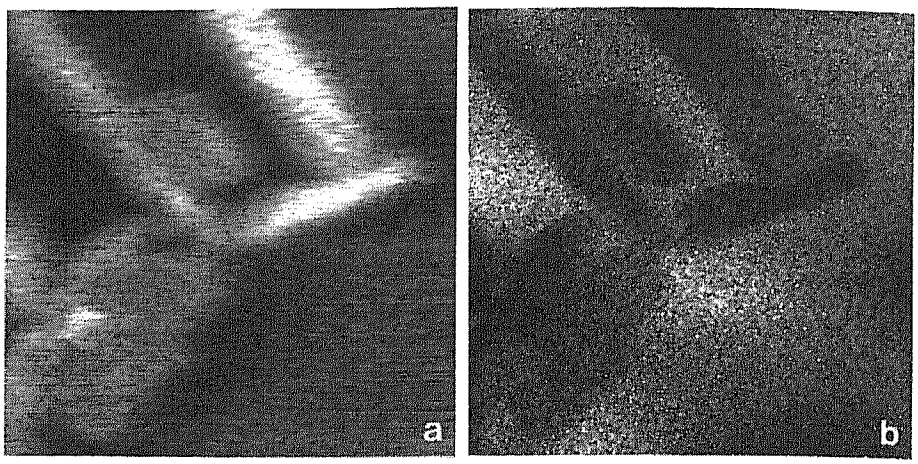

Figure 7. A 1 x 1 μm^2 scan of a 10,12-pentacosa-diynoic-acid (PCA) Langmuir-Blodgett monolayer on a glass substrate. (a) Force image displaying the topography of the 6 nm monolayer and (b) the simultaneously obtained PSTM image displaying absorption of the excitation at λ = 514 nm. Edge steepness of the optical contrast is 30 nm [21].

3.3. RIDGE WAVEGUIDES

Generally the contrast mechanism in PSTM is rather complicated because a combination of topographic effects, near field optical interactions and far field scattering is detected. Consequently contrast due to optical properties of the sample is only observed on samples with very shallow topography [19-21]. On the other hand for

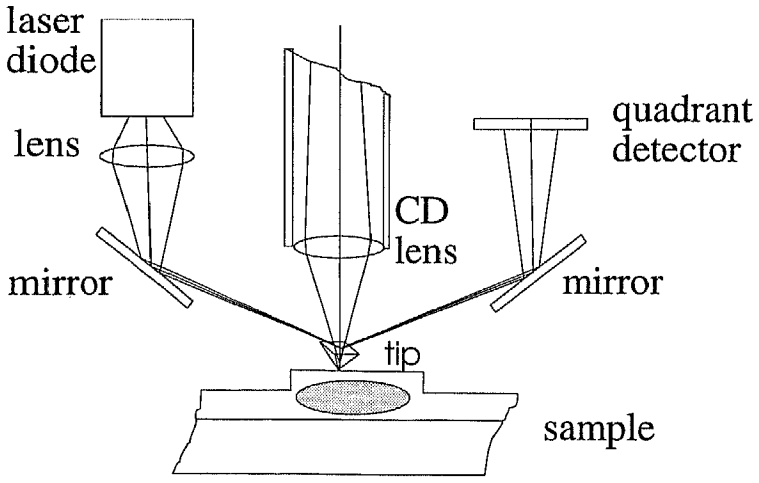

Figure 8. "Stand-alone" combined PSTM/AFM with SiN probe suitable for probing field distributions in integrated optical systems. The complete head, featuring force detection by optical beam deflection (laser diode, mirrors and quadrant detector) and optical detection via a compact-disc (CD) player lens, is mounted on a piezo-electric scanner with 100 x 200 μm^2 scan area.

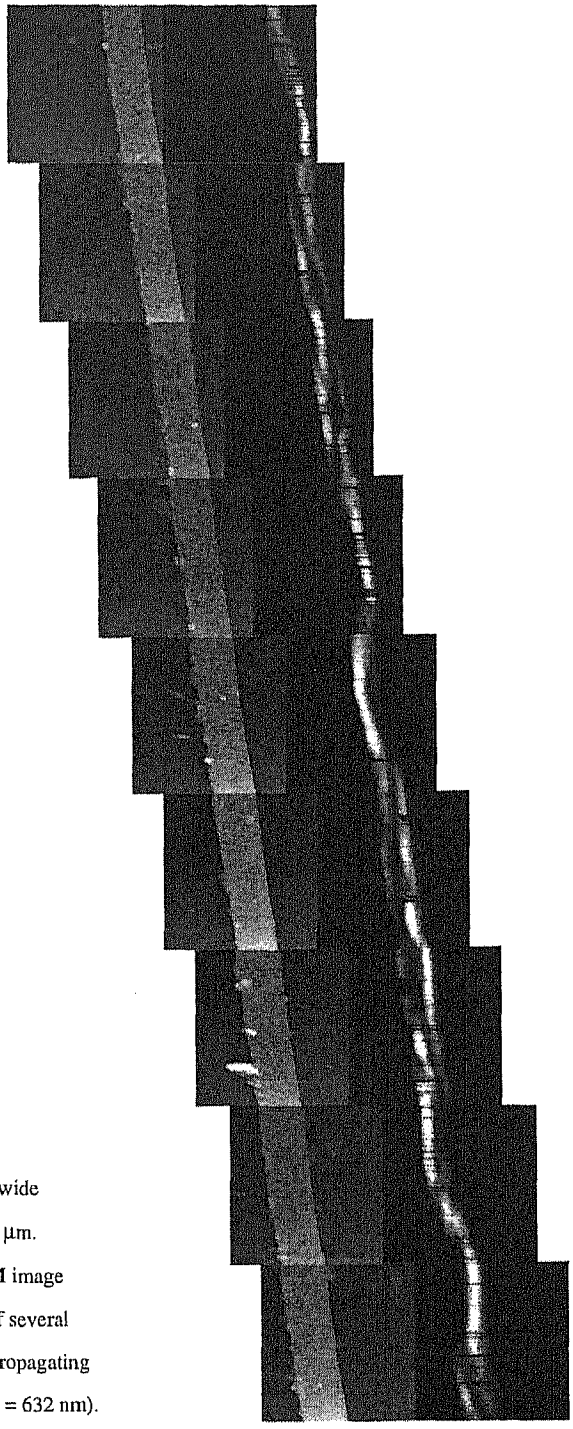

Figure 9.

Consecutive PSTM/AFM scans ($20 \times 40\ \mu m^2$) of a SiON ridge waveguide. *Left:* AFM image showing the topography of the ridge, 100 nm in height and 5 μm wide over a total length of 360 μm. *Right:* Corresponding PSTM image showing the beat pattern of several waveguide modes while propagating along the optical channel ($\lambda = 632$ nm).

the ideal case of total internal reflection at a glass-air transition the PSTM signal shows good quantitative correspondence with the evanescent field distribution following Fresnell equations. Consequently PSTM is an appropriate technique to study systems which display pure evanescent waves, i.e. ideal for application to optical waveguide systems. This potential was first explored by Tsai *et al.* [22] using fibre probes. Here we present the first results of combined PSTM/AFM applied to integrated optical waveguides.

Coupling of laser light to integrated optical waveguide by prism coupling, end-fire coupling or fibre coupling is rather critical and does not allow the waveguide to be scanned for microscopy. Consequently we have developed a "stand-alone" combined PSTM/AFM by scanning the SiN probe. The set-up is sketched in Figure 8. the microscope head is miniaturised using a compact-disc player lens (5 mm focus, 0.4 NA) for light collection, a miniature PMT (Hamamatsu R5600) for detection, and by folding the optical beam deflection detection system in a U-shape around the light collection path. The complete head is mounted on a piezo-electrical scanner with (100 x 200 μm^2 range), which rests on a tripod mechanical approach system.

Figure 9 clearly illustrates the advantage of the "stand-alone" PSTM/AFM. The image shows a SiON waveguide fabricated by pressure enhanced CVD on a thermally oxidised Si-wafer. The SiON ridge, 5 μm wide and 100 nm high, was fabricated using standard photolithographic techniques. The AFM image to the left displays the ridge topography and some dust particles. The PSTM image to the right displays the field distribution of end-fire coupled HeNe-laser light. The presence of several modes can be recognised in the mode beat pattern winding along the waveguide. The "stand-alone" feature allows concatenation of several scans, without affecting the in-coupling conditions. Thus in Figure 9 a beat period of 300 μm can be found, indicating two modes with 0.0021 difference in effective refractive index. It should be noted that the scans have a 1:2 aspect ratio in order to magnify the ridge area.

The combination of excited waveguide modes can be selected by changing the coupling conditions. This is illustrated in Figure 10. A Y_2O_3 waveguide is shown, with 100 nm step height, 8 μm width, over 100 μm length. Laser diode radiation, $\lambda = 1.48$ μm, is coupled in and detected using a Ge photo-diode. For low NA coupling only TM0 and TM1 mode are excited (Fig. 10b), while for high NA TM-modes up to TM3 are excited (Fig. 10d). Comparison of corresponding AFM and PSTM scans shows that the ridge edges cause a dark line in the PSTM images. Interestingly also the extend of the optical field beside the ridge dimension can be seen. For a quantitative interpretation of the PSTM images we have calculated the field distribution using the finite difference beam propagation method (BPM) [23]. In Figure 11 the PSTM image of the Y_2O_3 waveguide is presented together with simulated image for combined TM0, TM1 and TM3 excitation. The beat patterns show similarities, however the beat period in the simulation is 1.8 times the observed value. The same discrepancy was found comparing other mode combinations.

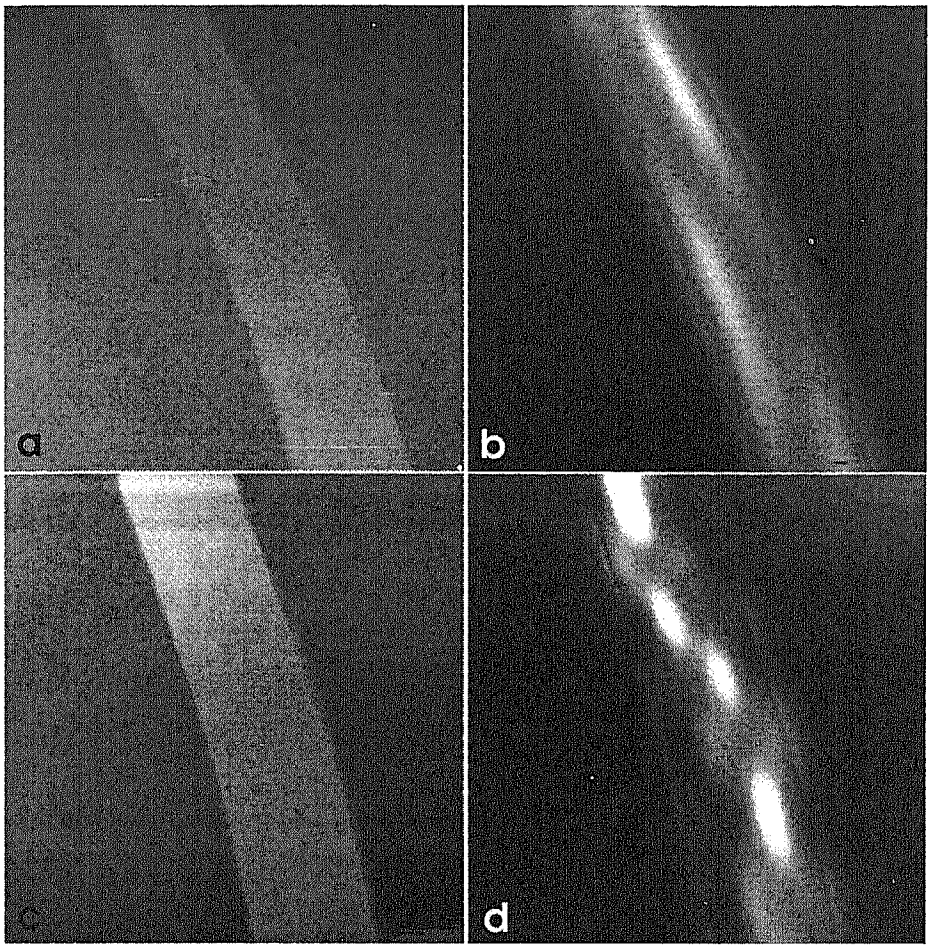

Figure 10. PSTM / AFM scans of a Y_2O_3 waveguide (100 nm step height, 8 μm width) for different TM modes at λ = 1.48 μm. (a) Topography of the Y_2O_3 ridge, 100 μm long, by AFM; (b) corresponding PSTM image with mode beat between TM0 and TM1 modes; (c) topography; (d) PSTM image with TM modes up to TM3.

Up to now field distributions in the lateral direction were presented. By approaching the SiN probe towards the waveguide the extend of the evanescent wave in the vertical direction can be probed. This is shown in Figure 12 for the Y_2O_3 waveguide for TE0 and TM0 mode. The field decays exponentially with the vertical distance. The decay length is in good agreement with the calculated value from the effective index for both modes (see Fig. 12). The TM-mode is more outspread, as expected, and gives a higher PSTM signal due to the higher field at the waveguide surface and the more favourable boundary conditions for this polarisation condition.

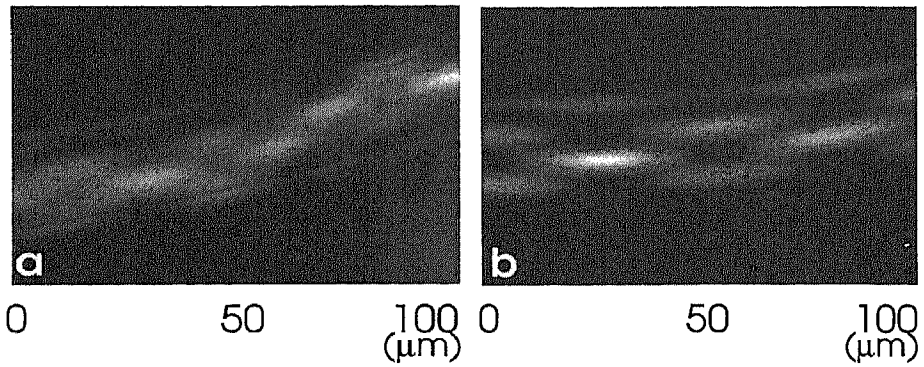

Figure 11. Comparison of the field distribution in a Y_2O_3 channel waveguide (100 nm step height, 8 μm width) at $\lambda = 1.48$ μm, (a) as observed by PSTM and (b) as simulated by the finite difference beam propagation method (BPM).

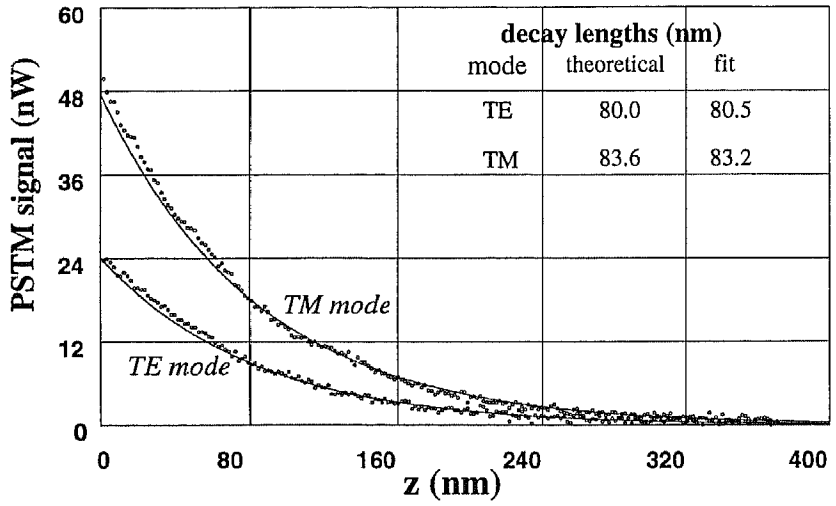

Figure 12. PSTM signal as a function of the distance of the SiN probe to a Y_2O_3 waveguide, for TE0 and TM0 mode. Solid lines are a single exponential decay as fitted to the experimental data. In the table the fitted decay length is given together with the theoretical value as calculated from the effective index for TE and TM mode, respectively.

Finally application of PSTM/AFM to a Y-junction is presented. The field distribution in the junction is affected by reflection or scattering at the splitting point, resulting in characteristic interference patterns. Clearly the performance of the Y-junction is strongly determined by the behaviour at this critical point. Notice the dust particles appearing as dark spots in the optical image.

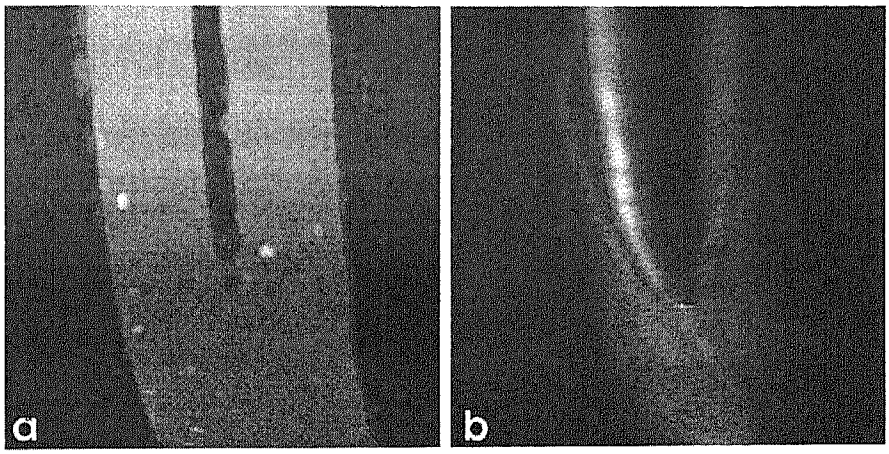

Figure 13. Corresponding (a) AFM and (b) PSTM image of a 15 x 40 μm^2 area of a Y-junction in SiON, with HeNe laser light (λ = 632 nm) propagating from bottom to top.

4. Conclusions

We have presented applications of two near field optical techniques, both in combination with force microscopy. Aperture SNOM with fluorescence detection gives (bio)chemical specificity and orientational information, down to single molecular sensitivity, in addition to the simultaneously acquired force image. We have shown that DNA sequencing and molecular organisation in mono-layers are interesting application fields. PSTM gives a direct mapping of optical waveguide field distributions, both in lateral and vertical direction, which allows detailed analysis of the performance of integrated optical devices.

5. Acknowledgements

The authors thank Wouter Kalle and Joop Wiegant of RijksUniversiteit Leiden for the preparation of in situ hybridised chromosomes, Uli Hoffmann and Hermann Gaub of the Technical University of Munich for the DPDA and PCA films, Eddy Schipper and Harm van Weerden for the Y-junctions and Y_2O_3 waveguides, and Ton Ruiter, Frans Segerink, Eric Schipper, Kees van der Werf, Ine Segers and Bart de Grooth for their assistance and suggestions. This research is mainly supported by the Dutch Foundation for Fundamental Research (FOM, project 91.942).

6. References

1. Pohl, D.W., Denk, W. and Lanz, M. (1984) Optical stethoscopy: image recording with resolution λ/20, *Appl. Phys. Lett.* **44**, 651-653.
2. Betzig, E., Trautman, J.K., Harris, T.D., Weiner, J.S. and Kostelak, R.L. (1991) Breaking the Diffraction Barrier: Optical Microscopy on a Nanometric Scale, *Science* **251**, 1468-1470.
3. Betzig, E. and Trautman, J.K. (1992) Near-field optics: microscopy, spectroscopy and surface modification beyond the diffraction limit, *Science* **257**, 189-195.
4. Toledo-Crow, R., Yang, P.C., Chen, Y. and Vaez-Iravani, M. (1992) Near-field differential scanning optical microscope with atomic force regulation, *Appl. Phys. Lett.* **60**, 2957-2959.
5. Betzig, E., Finn, P.L. and Weiner, J.S. (1992) Combined shear force and near-field scanning optical microscopy, *Appl. Phys. Lett.* **60**, 2484-2486.
6. Betzig, E. and Chichester, R.J. (1993) Near-field Fluorescence Imaging of Cytoskeletal Actin, *Bioimaging* **1**, 129-133.
7. Moers, M.H.P., Gaub, H.E. and Van Hulst, N.F. (1994) Poly(diacetylene) Monolayers Studied with a Fluorescence Scanning Near-Field Optical Microscope, *Langmuir* **10**, 2774-2777.
8. Betzig, E. and Chichester, R.J. (1993) Single Molecule observed by Near field Scanning Optical Microscopy, *Science* **262**, 1422-1425.
9. Trautman, J.K., Macklin, J.J., Brus, L.E. and Betzig, E. (1994) Near field spectroscopy of single molecules at room temperature, *Nature* **369**, 40-42.
10. Hess, H., Betzig, E., Harris, T.D., Pfeiffer, L.N. and West, K.W. (1994) Near-field spectroscopy of the quantum constituents of a luminescent system, *Science* **264**, 1740-1745.
11. Sunney Xie, X. and Dunn, R.C. (1994) Probing Single Molecule Dynamics, *Science* **265**, 361-364.
12. Ambrose, W.P., Goodwin, P.M., Martin, J.C. and Keller, R.A. (1994) Alterations of Single Molecule Fluorescence Lifetimes in Near-Field Optical Microscopy, *Science* **265**, 364-367.
13. Moers, M.H.P., Ruiter, A.G.T., Van Hulst, N.F. and Bölger, B. (jan. 1995) Optical contrast in Near-Field Techniques, *Ultramicroscopy*, Proceedings International Conference on Near field Optics II, Raleigh NC, Oct 1993, in press.
14. Tillmann, R.W., Radmacher, M., Gaub, H.E., Kenney, P. and Ribi, H.O. (1993) *J. Phys. Chem.* **97**, 2928-2932.
15. Rudkin, G.T. and Stollar, B.D. (1977) High resolution detection of DNA-RNA hybrids in situ by indirect immunofluorescence, *Nature* **265**, 472-473.
16. Bauman, J.G.J., Wiegant, J. and Van Duijn, P. (1981) Cytochemical hybridisation with fluorochrome-labeled RNA, *J. Histochem. Cytochem.* **29**, 227-246.
17. Wiegant, J., Wiesmeijer, C.C., Hoovers, J.M.N., Schuuring, E., d'Azzo, A., Vrolijk, J., Tanke, H.J. and Raap, A.K. (1993) Multiple and sensitive fluorescence in situ hybridisation with rhodamine-, fluorescein-, and coumarin-labelled DNAs, *Cytogenetics and Cell Genetics* **63**, 73-76.
18. Putman, C.A.J., De Grooth, B.G., Wiegant, J., Raap, A.K., Van der werf, K.O., Van Hulst, N.F. and Greve, J. (1993) Detection of In Situ Hybridization to Human Chromosomes with the Atomic Force Microscope, *Cytometry* **14**, 356-361.
19. Van Hulst, N.F., Moers, M.H.P., Noordman, O.F.J., Tack, R.G., Segerink, F.B. and Bölger, B. (1993) Near-field optical microscope using a silicon-nitride probe, *Appl. Phys. Lett.* **62**, 461-463.
20. Van Hulst, N.F., Moers, M.H.P. and Bölger, B. (1993) Near-field optical microscopy in transmission and reflection modes in combination with force microscopy, *J. Microscopy.* **171**, 95-105.
21. Moers, M.H.P., Tack, R.G., Van Hulst, N.F. and Bölger, B. (1994) Photon scanning tunneling microscope in combination with a force microscope, *J. Appl. Phys.* **75**, 1254-1257.
22. Tsai, D.P., Jackson, H.E., Reddick, R.C., Sharp, S.H. and Warmack, R.J. (1990) Photon scanning tunneling microscope study of optical waveguides, *Appl. Phys. Lett.* **56**, 1515-1517.
23. Hoekstra, H.J.W.M., Krijnen, G.J.M. and Lambeck, P.V. (1993) New formulation of the beam propagation method, *Opt. Commun.* **97**, 301-303.